RSC Advances

PAPER

View Article Online
View Journal | View Issue

Cite this: *RSC Adv.*, 2025, **15**, 37876

Green diesel production *via* deoxygenation of triolein catalysed by nickel-molybdenum-supported catalysts

G. AbdulKareem-Alsultan, *[a] Nur Athirah Adzahar,[a] G. Omer-Alsultan,[a] N. Asikin-Mijan, *[b] H. V. Lee, [c] Tonni Agustiono Kurniawan[d] and Y. H. Taufiq-Yap *[a]

The deoxygenation of triolein into hydrocarbons has been carried out over NiO/CeO_2, MoO_2/CeO_2 and $NiO–MoO_2/CeO_2$ under partial vacuum and solvent-free conditions. $NiO–MoO_2/CeO_2$ exhibited a remarkably higher yield of hydrocarbons (65%) and n-C_{17} selectivity (37%) in comparison with single metal oxide–supported CeO_2 catalysts. Interestingly, the rich acid–base character and excellent synergistic effect between Ni–Mo and CeO_2 positively impacted the deoxygenation reaction while suppressing the cracking reaction. The addition of Ni- and Mo-rich species deteriorated the deoxygenation activity. The highest hydrocarbon yield (77%) and n-C_{17} selectivity (58%) can be achieved at a reaction temperature of 340 °C, 1 h of reaction time, 15 wt% of catalyst loading and 10 mbar of reaction pressure under partial vacuum conditions. Based on catalyst support comparison (CeO_2, Al_2O_3, SiO_2, and ZSM-5), CeO_2 is a promising catalyst support for the production of diesel-rich fuels *via* solvent-free catalytic deoxygenation of triolein.

Received 4th July 2025
Accepted 2nd September 2025

DOI: 10.1039/d5ra04601g

rsc.li/rsc-advances

1. Introduction

Petroleum-based fuels are the major source of energy for transportation but have a limited and non-renewable source. Due to the drastic depletion of petroleum reserves and increasing global climate change,[1] the production of biofuels from renewable resources is of great demand. For instance, biofuel-derived fatty acid methyl esters (FAMEs) are the most common biofuels being used.[2,3] Nonetheless, the oxygenated species in FAMEs lead to severe engine complications such as corrosion of metal parts, filter plugging and deposits on fuel pumps.[4] Hence, the production of oxygen-free biofuels has gained great interest. Green diesel, which is an oxygen-free hydrocarbon-based fuel, can be obtained *via* deoxygenation (DO) of various non-fossil resources.[5] The deoxygenation process is a route related to the cracking of hydrocarbon chains, and the oxygen species can be removed in the form of CO_2/CO *via* decarboxylation/decarbonylation pathways.

In recent years, various types of acid catalysts, including noble-metal–supported catalysts (*e.g.*, Ni, Pd, and Pt),[6] Mo-based sulfide catalysts (*e.g.*, $CoMoS_x$ and $NiMoS_x$),[1] mesoporous TiO_2 (ref. 7) and mesoporous Al_2O_3–TiO_2,[8] have been extensively studied by many researchers for the deoxygenation reaction. However, these catalysts suffer from drawbacks such as high noble metal cost, sulfur pollution risk, low catalyst acidity, and poor product selectivity. To overcome these drawbacks, efforts have been focused on the use of sulfur-free and low-cost catalysts for the production of high-quality green diesel *via* deoxygenation. Note that the combination of Ni with Mo has been found to be significantly effective for the conversion of triglycerides or fatty acid derivatives into fuels[9,10] and proven for oxygen removal activity. Recently,[11] the deoxygenation of vegetable oil over $NiMo/Al_2O_3$ was studied, and highest content of diesel range hydrocarbon was reported. Considerable attention has also been paid to hierarchical mesoporous materials such as ZSM-5 in a deoxygenation reaction, yet the majority of products obtained are gasoline-range hydrocarbons.[12] Indeed, the mesoporous character providing a faster diffusion of molecules can increase hydrocarbon yields.[13] Although many researchers have reported the performance of Ni–Mo supported onto mesoporous supports,[12,14,15] most H_2 co-feed hydrodeoxygenation reactions require pretreatment of catalysts in an H_2 atmosphere to reduce the oxide into a metallic form. Nevertheless, the utilisation of these catalysts in H_2-free deoxygenation has been rarely reported.

Cerium oxide (CeO_2) is an excellent catalyst additive that has been recently used in deoxygenation reactions. Note that CeO_2 is an acid–base oxide and possesses many oxygen vacancies.[6,16] The base character will allow greater oxygen removal from the

[a]*Catalysis Science and Technology Research Centre, Faculty of Science, Universiti Putra Malaysia, 43400 Serdang, Selangor, Malaysia*

[b]*Department of Chemical Sciences, Faculty of Science and Technology, Universiti Kebangsaan Malaysia, 43600 UKM Bangi, Selangor Darul Ehsan, Malaysia*

[c]*Nanotechnology and Catalysis Research Centre (NanoCat), Universiti Malaya, 50603 Kuala Lumpur, Malaysia*

[d]*College of the Environment and Ecology, Xiamen University, Xiamen 361102, Fujian, China*

reactant (absorb more CO_2 in the gas phase) and suppress the coking with the increase in H/C ratio.[17] Meanwhile, the acid character will favour the C–C bond cleavage, and the oxygen vacancies are beneficial for ester group activation.[18] Additionally, CeO_2 exhibits outstanding redox properties, enabling the continuous generation of oxygen vacancy sites during the reaction. These vacancies significantly enhance the material's affinity for oxygen removal.[19,20] This phenomenon was recently corroborated by a study employing a Ni–Cu supported CeO_2 catalyst, which showed excellent oxygenate removal activity through the hydrodeoxygenation reaction.[21] Indeed, the effectiveness of CeO_2 is attributed to the additional activation of oxy-compounds on the CeO_2 surface. Similar results were observed by Aliana-Nasharuddin *et al.* (2019) at a temperature of 350 °C, in which the supported Ni–Ce catalyst was found to be active and rising the formation of hydrocarbon-rich product. Noteworthy, superior deoxygenation activity is also strongly correlated with excellent metal dispersion.[22] The implementation of nano-sized CeO_2 is ideally desirable for this task in which the high surface area of nanosized CeO may render greater dispersion of the active metal. Therefore, the present study focused on the development of Ni–Mo supported onto CeO_2 and further compared it with various mesoporous supports (SiO_2, Al_2O_3 and ZSM-5) for solventless and H_2-free deoxygenation of triolein.

Our study successfully demonstrated a solvent-free and H_2-free pathway for the deoxygenation of triolein under partial vacuum conditions, thereby lowering process complexity, environmental risk, and cost. The novelty lies in developing and systematically evaluating a bimetallic NiO–MoO_2 catalyst supported on nanostructured CeO_2 (NiO–MoO_2/CeO_2), which to the best of our knowledge has not been comprehensively reported before for this application. The nanosized CeO_2 support provides high surface area, abundant oxygen vacancies, and strong acid–base properties, which synergistically interact with Ni and Mo species to enhance the C–O bond cleavage while suppressing undesired cracking reactions. This unique acid–base synergy is further proven by our TPD-NH_3 and TPD-CO_2 analyses, which reveal a significantly higher density of weak acid–base sites than single-metal catalysts. Second, our work demonstrates unprecedented catalytic performance, achieving a hydrocarbon yield of 77% and an *n*-C_{17} selectivity of 58% under optimized conditions (15 wt% catalyst loading, 340 °C, 1 h, 10 mbar). These values surpass the majority of previously reported non-noble, sulfur-free catalytic systems. Another original contribution is our detailed comparison of different supports (CeO_2, Al_2O_3, SiO_2, and ZSM-5), which establishes CeO_2 as the most effective support for maximizing *n*-C_{17} selectivity and minimizing light hydrocarbon fractions, offering new insights into support–metal interactions for biofuel upgrading. Furthermore, by systematically varying the Ni/Mo ratio, we showed that a balanced 10 : 10 composition outperforms Ni- or Mo-rich systems, a critical finding for future catalyst designs, as excessive Ni promotes cracking while excessive Mo suppresses desired decarboxylation/decarbonylation pathways. Moreover, our work supplies mechanistic insights into how CeO_2 vacancies facilitate deoxygenation through redox character and oxygen affinity, enriching the fundamental understanding of catalytic performance in H_2-free environments. Crucially, the process involves no external hydrogen or solvent, which renders it more industrially viable and environmentally benign, in that CO_2 footprint is diminished while sulfur poisoning due to conventional sulfided catalysts is evaded. The combined innovations underscore the significance of our research in introducing a new generation of non-noble, sulfur-free, nanoscale CeO_2-supported bimetallic catalysts for the facile production of diesel-range hydrocarbons *via* the deoxygenation of triglycerides. By quashing the dual challenge in the efficiency of catalysts as well as the sustainability of processes, our study not only enriches the scientific understanding in the field in relation to catalyst–support synergy in deoxygenation, but also creates avenues towards large-scale, environmentally friendly production technologies for biofuels that are in tandem with energy transition objectives globally.

2. Experimental

2.1 Catalyst preparation

In this study, various catalyst supports were used to prepare catalysts such as ceria oxide nanopowder (CeO_2; purity of 99.9%, Sigma-Aldrich, USA), alumina oxide (Al_2O_3; purity of 99.9%, BDH, England), ZMS-5 ($SiO_2/Al_2O_3 = 38$, SBET = 710 m^2 g^{-1}, Alfa Aesar, MA) and silica gel 60 high-purity grade (Merck KGaA, Germany). The binary metal oxide–supported catalysts were prepared *via* an impregnation method with a fix ratio of Ni/Mo (10/10). Prior to the impregnation, about 0.73 g of nickel(II) hexahydrate ($Ni(NO_3)_2 \cdot 6H_2O$; purity of 99%, Merck KGaA, Germany) and about 0.73 g of ammonium heptamolybdate tetrahydrate ($(NH_4)_6Mo_7O_{24} \cdot 4H_2O$; purity of 99%, Merck KGaA, Germany) were mixed and dissolved in 15 mL of distilled water. The metal salt mixture was impregnated onto about 3.01 g of CeO_2 nanopowder and continuously stirred for 4 h (400 rpm), followed by drying for 48 h, grinding and calcination at 400 °C for 4 h under atmospheric conditions. The catalyst is denoted as NiO–MoO_2/CeO_2. Notably, CeO_2 has also been used to support single metal oxides, such as NiO and MoO_2, yielding NiO/CeO_2 and MoO_2/CeO_2 catalysts. Furthermore, a similar impregnation technique was employed using other types of supports such as silica gel 60, ZMS-5 and Al_2O_3 to produce the NiO–MoO_2/SiO_2, NiO–MoO_2/ZSM-5 and NiO–MoO_2/Al_2O_3 catalysts. The effect of Ni : Mo loading was also further investigated by varying the ratio at 5/15, 10/10, and 15/5, and the prepared catalysts were denoted as 5NiO : 15MoO_2, 10NiO : 10MoO_2 and 15NiO : 5MoO_2.

2.2 Catalyst characterisation

The X-ray diffraction (XRD) patterns of the catalysts were acquired using a Shimadzu diffractometer (model XRD-6000) with CuK_α radiation generated by a Philip glass diffraction X-ray tube (a broad focus of 2.7 kW type) at a scanning rate of 2° min^{-1} over a 2θ range of 10°–70°. The acidity and basicity properties were determined by temperature-programmed desorption of ammonia (TPD-NH_3) and temperature-programmed desorption of carbon dioxide (TPD-CO_2), using

a Thermo Finnigan TPD/R/O 1100 instrument equipped with a thermal conductivity detector (TCD). For the acidity measurement using TPD-NH_3, approximately 0.05 g of catalyst was placed in a quartz U-tube. Before the adsorption, the catalyst was pretreated in a flow of N_2 (20 mL min^{-1}) at 250 °C for 30 min. Subsequently, the catalyst was exposed to NH_3 for 1 h to allow the adsorption of NH_3 onto the catalyst surface. The excess of NH_3 was removed by 1 h through N_2 purging. The treated catalyst was further heated in a flow of He from 50 °C to 900 °C, ramping at 15 °C min^{-1}. For the basicity measurement using TPD-CO_2, the CO_2 adsorption and desorption were analyzed following a procedure similar to the TPD-NH_3 method.

2.3 Catalytic deoxygenation

The deoxygenation of triolein (glyceryl trioleate, ~65 wt% purity, Sigma-Aldrich, USA) was carried out in a 250 mL three-necked round-bottom flask with mechanical stirring as a semi-batch reactor. Before each run, about 10 g of triolein and 5 wt% catalyst were added, and the system was stirred constantly while purging with flowing N_2 to remove all residual oxygen. The reactor was then evacuated to nearly 10 mbar, heated to the desired temperature, namely 340–350 °C, and then isothermally maintained for 1 h, when the pressure settled to around 10 mbar. Condensable volatiles were collected downstream using a water-cooled condenser (~16 °C) in a receiving vessel. The liquid product was sampled every 1 h and then characterized by gas chromatography-mass spectrometry (GC-MS) to obtain the fatty acid composition, as given in Table 1. This stage was important in order to promote the condensation of volatile species into the liquid form. The collected liquid product was evaluated by GC-FID (gas chromatography-flame ionization detector) analysis.

The decarboxylation and decarbonylation are among the main deoxygenation routes that are characteristic in that the oxygen is lost in gaseous by-products, therefore forming lineal hydrocarbon molecules structurally similar to diesel-range alkanes. These are conducted at high temperatures (typically between 300 and 350 °C) under the application of metal–supported catalysts, with the added benefit that very low or no external hydrogen required in comparison to hydrodeoxygenation. The end carboxyl group (–COOH) in the fatty acid is removed as carbon dioxide (CO_2) in the course of the decarboxylation pathway. The reaction shortens the carbon chain of product hydrocarbon by one carbon compared to that in the parent fatty acid. For instance, stearic acid (C18:0) undergoes decarboxylation to give heptadecane ($C_{17}H_{36}$) as in eqn (1):

$$C_{17}H_{35}COOH \rightarrow C_{17}H_{36} + CO_2 \quad (1)$$

By contrast, the process of decarbonylation undergoes the breakdown of carbonylic functionality, donating carbon monoxide (CO) and, under hydrogen-rich conditions, water (H_2O). Similar to the instance involving decarboxylation, this reaction generates a reduced hydrocarbon chain shortened from the parent fatty acid by one carbon in length, though with variant side products. Decarbonylation from stearic acid can be exemplified by eqn (2):

$$C_{17}H_{35}COOH \rightarrow C_{17}H_{36} + CO + H_2O \quad (2)$$

Both processes produce long-chain *n*-alkanes that form the backbone of renewable diesel, but they vary in carbon efficiency and their environment impacts. Decarboxylation releases CO_2, which is a greenhouse gas emission source, while decarbonylation generates poisonous CO that can be valorized as part of a syngas. Selectivity between these two processes can be controlled catalytically by parameters such as hydrogen partial pressure, reactor type, and catalyst type.

Table 1 Physicochemical properties of triolein

Properties (%)	Triolein	Method
Acid value (mg KOH per g)	5.0	AOCS Ca 5a-40
FFA value (%)	2.5	AOCS Ca 5a-40
Fatty acid composition (%)		
Myristic acid (C14:0)	1.2	
Palmitic acid (C16:0)	3.8	
Stearic acid (C18:1)	1.9	
Oleic acid (C18:1)	83.3	
Linolenic acid (C18:2)	0.4	

2.4 Characterisation of liquid products

A gas chromatograph (Shimadzu GC-14B) equipped with an HP-5 capillary column (length: 30 m × inner diameter: 0.32 mm × film thickness: 0.25 μm) with a flame ionisation detector (FID) operating at 300 °C was used to measure the deoxygenated liquid products and determined using alkane standards (C_8–C_{20}). The deoxygenated liquid product was diluted with GC-grade *n*-hexane for the yield analysis. The internal standard for the quantitative analysis was 1-bromohexane. About 1 μL of the sample was injected into a GC column at an operating temperature of 250 °C, and nitrogen served as a carrier gas. About 40 °C was set as the initial temperature of the oven and held for 6 min. Furthermore, the temperature further increased to 270 °C at a heating rate of 7 °C min^{-1}. A gas chromatography-mass spectrometer (GC-MS) (model SHIMADZU QP5050A) equipped with a non-polar DB-5HT column (length: 30 m × inner diameter: 0.32 mm × film thickness: 0.25 μm) with a splitless inlet was used to characterise triolein. Then, the feedstock was diluted with GC-grade *n*-hexane (purity >98%) to 100 ppm. The National Institute of Standards and Testing (NIST) library identified the fraction peaks from the GC-MS spectrum, and the identified primary products matched equal or higher than 95%. The total chromatographic peak area for the hydrocarbon fractions (yield %) and the selectivity of hydrocarbons were identified using a similar method previously reported in our research group studies.[23,24]

The yield of hydrocarbon C_8–C_{20} is defined as follows:

$$X(\%) = \frac{\sum n_o + \sum n_i}{\sum n_z} \times 100 \quad (3)$$

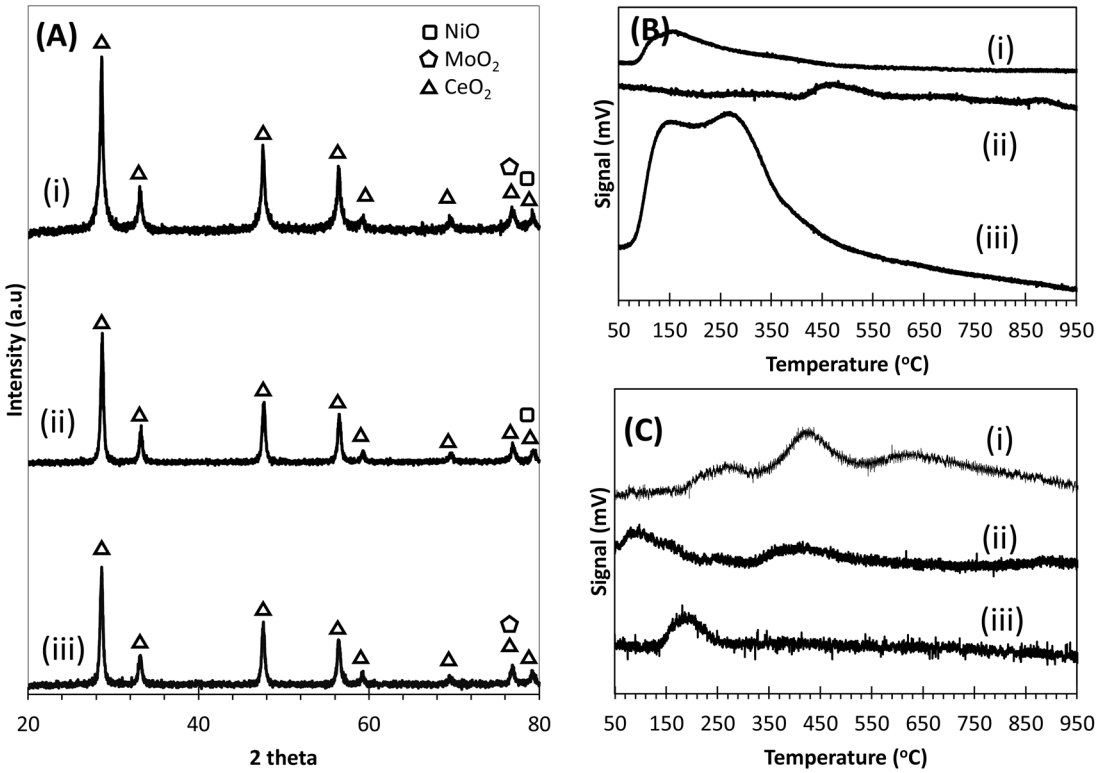

Fig. 1 (A) XRD patterns, (B) TPD-NH_3 and (C) TPD-CO_2 of (i) NiO–MoO_2/CeO_2, (ii) NiO/CeO_2, and (iii) MoO_2/CeO_2 catalysts.

where n_o is the peak area of alkenes (C_8–C_{20}), n_i is the peak area of alkanes, and n_z is the peak area of the product.

The hydrocarbon fraction selectivity is defined as follows:

$$S_x(\%) = \frac{C_x}{\sum n_x} \times 100 \quad (4)$$

where C_x is the peak area of hydrocarbon fraction and n_x is the total peak area of hydrocarbons.

3. Results and discussion

3.1 Catalyst characterisation

X-ray diffraction is used to study the structure and crystalline phase of catalyst. Fig. 1A shows the XRD patterns for NiO/CeO_2, MoO_2/CeO_2 and NiO–MoO_2/CeO_2 catalysts. The catalyst support, CeO_2, diffracted at 2θ of 28.55°, 33.09°, 47.48°, 56.34°, 59.09°, 69.1°, 76.81°, and 79.21° (JCPDS card no. 34-0394).[25,26] Note that the XRD peak belongs to NiO and MoO_2 appeared at 2θ of 79.21° (NiO: JCPDS card no. 01-072-1464) and 76.81° (MoO_2: JCPDS card no. 01-072-0527), as reported earlier.[27,28] All the catalysts were found to be well crystallised, as indicated by the intense XRD peaks. It is noteworthy to mention that successful incorporation of Ni and Mo oxide will result in intense peak formation at $2\theta = 43°$ for NiO and $2\theta = 26°$ and 37° for MoO_2, respectively. However, neither of these peaks were observed, indicating good dispersion of NiO and MoO_2 on CeO_2.[29,30] The crystallite size of the catalysts was determined using the Debye–Scherrer equation from CeO_2's main peak at $2\theta = 28.55°$. As shown in Table 2, the ranking of crystallite sizes is NiO–MoO_2/CeO_2 > NiO/CeO_2 > MoO_2/CeO_2. The trend suggests that the application of the combination of NiO and MoO_2 led to a slightly larger crystallite size than the single-component modifications. However, the differences between the three samples noticed in experiment are not that big, indicating that the deposition of NiO and MoO_2 species did not alter the inherent crystallite size of the CeO_2 support so much. In other

Table 2 Crystallite size and acid–basic properties of CeO_2-supported catalysts

	XRD	TPD			
Catalyst	Crystallite size (nm)	CO_2 desorption temperature (°C)	Basic sites (μmol g^{-1})	NH_3 desorption temperature (°C)	Acid sites (μmol g^{-1})
NiO–MoO_2/CeO_2	24	372/724	726/1264	202	4816
NiO/CeO_2	21	139/456	75/47	520	242
MoO_2/CeO_2	20	174	151	460	148

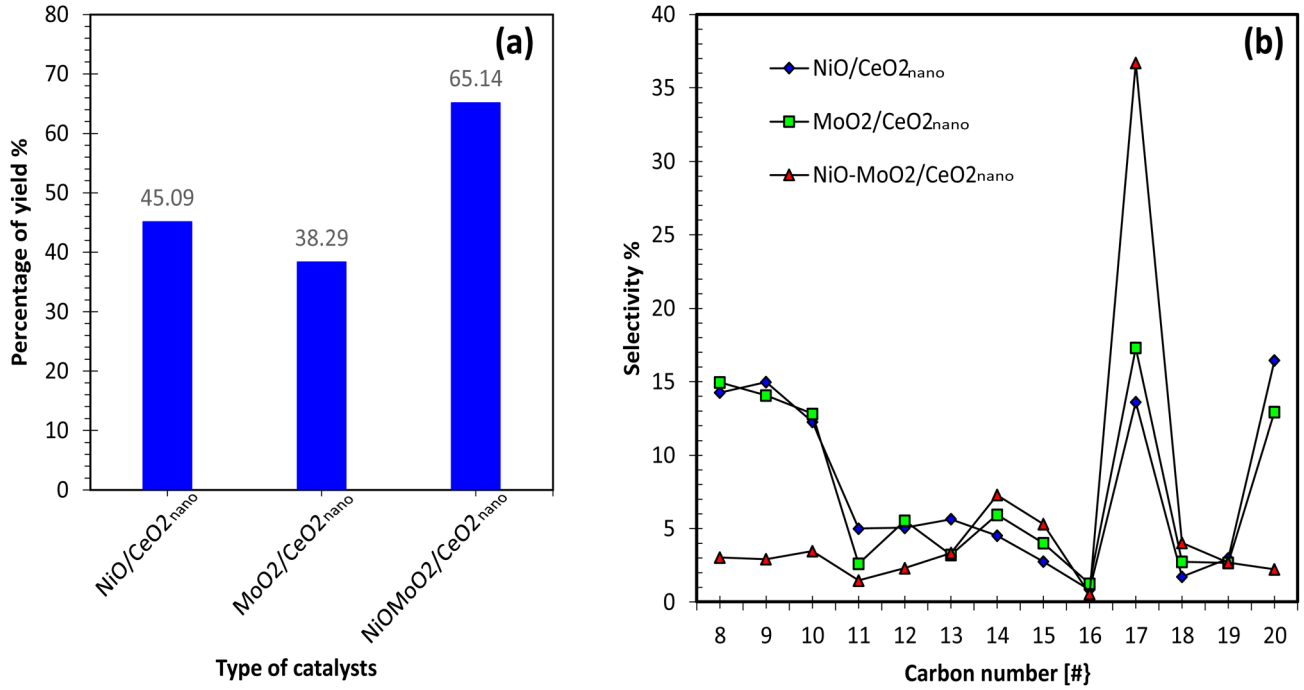

Fig. 2 (a) Hydrocarbon yield and (b) hydrocarbon distribution from the deoxygenation of triolein over CeO_2-supported catalysts.

words, the nanoscale structure of CeO_2 remained almost intact, which indicates that the support is stable against extensive crystal growth even after modification.

Temperature-programmed desorption (TPD) using NH_3 and CO_2 was conducted to examine the surface basicity and acidity of the catalysts, and the related profiles are presented in Fig. 1B and C. In all cases, desorption peaks at 50–200 °C, 200–500 °C, and 500–800 °C corresponded to weak, medium, and strong active sites, respectively. As can be seen from NH_3-TPD information (Table 2), the single metal oxide–supported catalysts (NiO/CeO_2 and MoO_2/CeO_2) exhibited largely medium and strong acid sites, but the sum of acid site densities for both was relatively low at ~148–242 μmol g^{-1}. The binary oxide catalyst ($NiO–MoO_2/CeO_2$), however, demonstrated a noteworthy increase in total acidity to 4816 μmol g^{-1}, with the majority of sites belonging to the weak category. This remarkable enhancement is the effect of the synergistic interaction between NiO, MoO_2, and the CeO_2 support, which brought higher numbers of available acid sites on the surface of the catalyst. The findings therefore illustrate that while individual-oxide supports assist in the provision of moderate acidity, the cooperative effect among the bimetallic system increases significantly the density of acid sites, an area that can play a very vital role in catalytic activity as well as stability.[10] Similar trends can be observed for the TPD-CO_2 of all the catalysts. Again, $NiO–MoO_2/CeO_2$ gave the strongest basic active site with the highest density, as tabulated in Table 2. The active acid–base sites of the catalyst will promote the C–C and C–O bond cleavages. These can be achieved by cracking, decarboxylation and decarbonylation pathways. The basicity of the catalyst also suppressed the coke deposition.[22] Therefore, among the catalysts, $NiO–MoO_2/CeO_2$ is predicted to be highly favorable for the occurrence of deoxygenation reactions.

3.2 Catalytic deoxygenation activities

Catalytic deoxygenation of triolein was performed under partial vacuum conditions at 340 °C and 10 mbar for 1 h. The deoxygenation activity reported in terms of hydrocarbon yield is shown in Fig. 2a. It had found that the highest hydrocarbon yield can be obtained using $NiO–MoO_2/CeO_2$ followed by NiO/CeO_2 and MoO_2/CeO_2. The binary metal oxide–supported CeO_2 catalyst transformed triolein to 65% of hydrocarbon liquid fuel. Based on Table 1, triolein is mainly composed of oleic acid (C18 : 1). Upon deoxygenation, this fatty acid will convert into *n*-C_{17} (*n*-heptadecene or *n*-heptadecane). Indeed, the $NiO–MoO_2/CeO_2$ catalyst was highly selective towards the *n*-C_{17} product ranging from 15% to 37% (Fig. 2b). However, the single metal oxide–supported CeO_2 catalysts only exhibited about 15–18% of *n*-C_{17} hydrocarbon. The highest *n*-C_{17} selectivity by the $NiO–MoO_2/CeO_2$ catalyst confirmed that the acid–base active sites and excellent synergistic effect between Ni and Mo on CeO_2 are important for promoting the decarboxylation and decarbonylation reactions.[31,32]

3.3 Optimisation of deoxygenation activities

As explained, the $NiO–MoO_2/CeO_2$ catalyst gave the highest deoxygenation activity, with 65% of hydrocarbon yield and 37% of selectivity towards *n*-C_{17}. Hence, the deoxygenation of triolein with the same catalyst also optimised using one-variable-at-a-time (OVAT) technique, and the obtained results are shown in Fig. 3a–f.

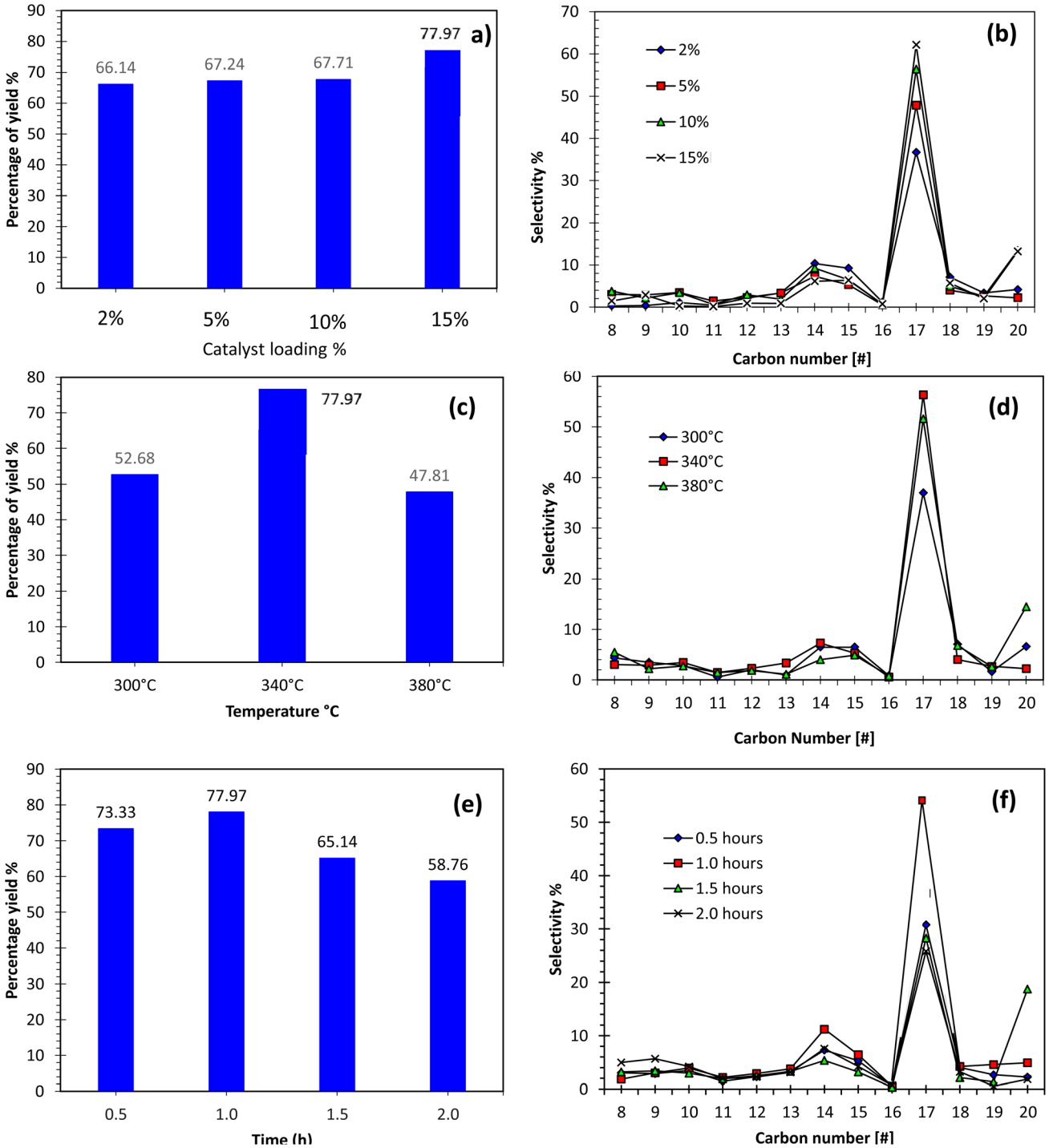

Fig. 3 Optimization studies of triolein deoxygenation: (a and b) effect of catalyst amount (reaction condition: 340 °C, 10 mbar, 1 h, and 400 rpm), (c and d) effect of reaction temperature (reaction condition: 15 wt% catalyst, 10 mbar, 1 h, and 400 rpm), and (e and f) effect of reaction time (reaction condition: 340 °C, 10 mbar, 15 wt% catalyst, and 400 rpm).

The effects of catalyst loading (5–15 wt%) on the hydrocarbon yield and product selectivity at 340 °C, 40 min reaction time, under partial vacuum conditions of 10 mbar reaction pressure, and 400 rpm stirring rate are shown in Fig. 3a and b. Based on the result, increasing the catalyst loading from 5 to 15 wt% led to an increase in hydrocarbon yield and C_{17} selectivity, as the optimum hydrocarbon yield (71.55%) with selectivity towards C_{17} (62.13%) was obtained with 15 wt% NiO–MoO_3/CeO_{2nano}. This is because increasing the catalyst loading led to more catalyst active sites being available for the deoxygenation reaction.[33,34] However, 5 wt% catalyst loading was chosen as the best condition, even though 15 wt% showed the

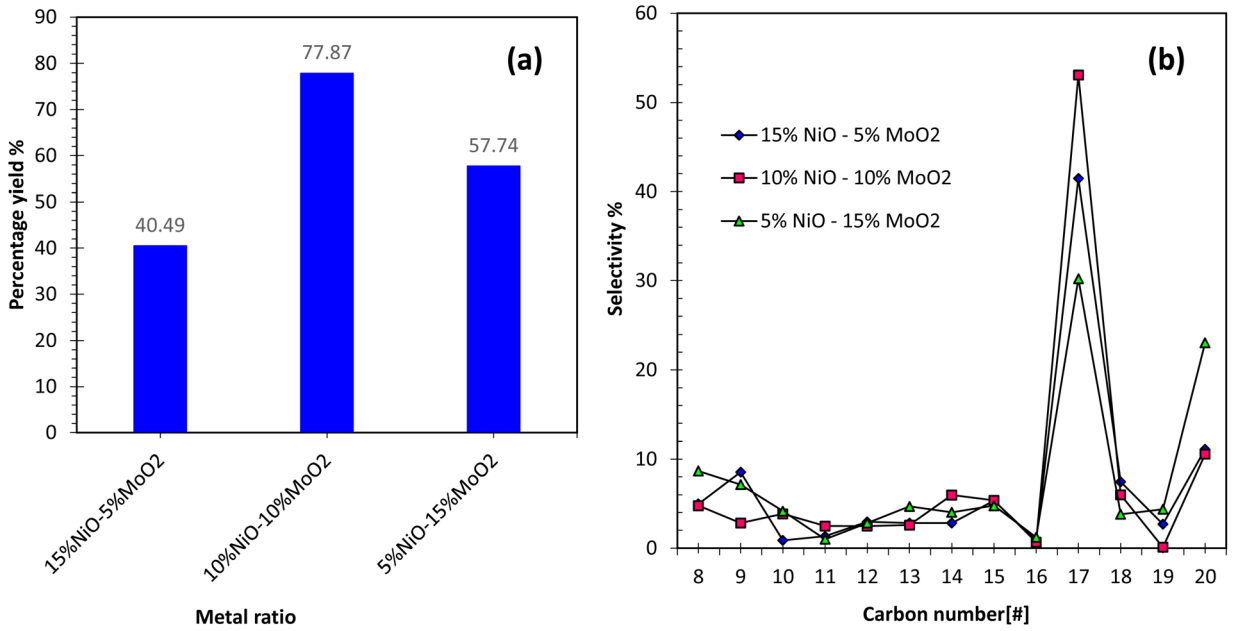

Fig. 4 Effect of Ni/Mo ratio on the deoxygenated liquid product: (a) hydrocarbon yield and (b) hydrocarbon distribution. Reaction conditions: 340 °C, 10 mbar, 15 wt%, 1 h, and 400 rpm.

highest hydrocarbon yield, but the increment in the yield is too small, which is from 67.24% to 71.55% only.

The effects of catalyst loading (2–15 wt%) on the hydrocarbon yield and product selectivity were studied. The resulting products increased with the increase in catalyst loading due to the higher amount of active sites present in the catalyst, which promoted the deoxygenation reaction.[35] It revealed that a high catalyst loading is required to obtain the *n*-C_{17}-rich product. The effect of reaction temperature was also studied. The deoxygenation activity followed the order of 340 °C > 300 °C > 380 °C. The formation of hydrocarbons increased as the temperature increased, and a significant reduction can be noticed beyond 340 °C because the deoxygenated hydrocarbon product was further cracked to gaseous products. Besides, the polymerisation reaction can occur at a high reaction temperature. As evinced in Fig. 3d, the polymerised *n*-C_{20} noticeable at 380 °C suggested that a high reaction temperature favoured the polymerisation reaction. It is worthy of mentioning that *n*-C_{17} was highly selective at the lowest temperature (300 °C), indicating that the removal of oxygenated species *via* decarboxylation/decarbonylation is effective at a lower reaction temperature. Next, the effect of reaction time on the catalytic deoxygenation

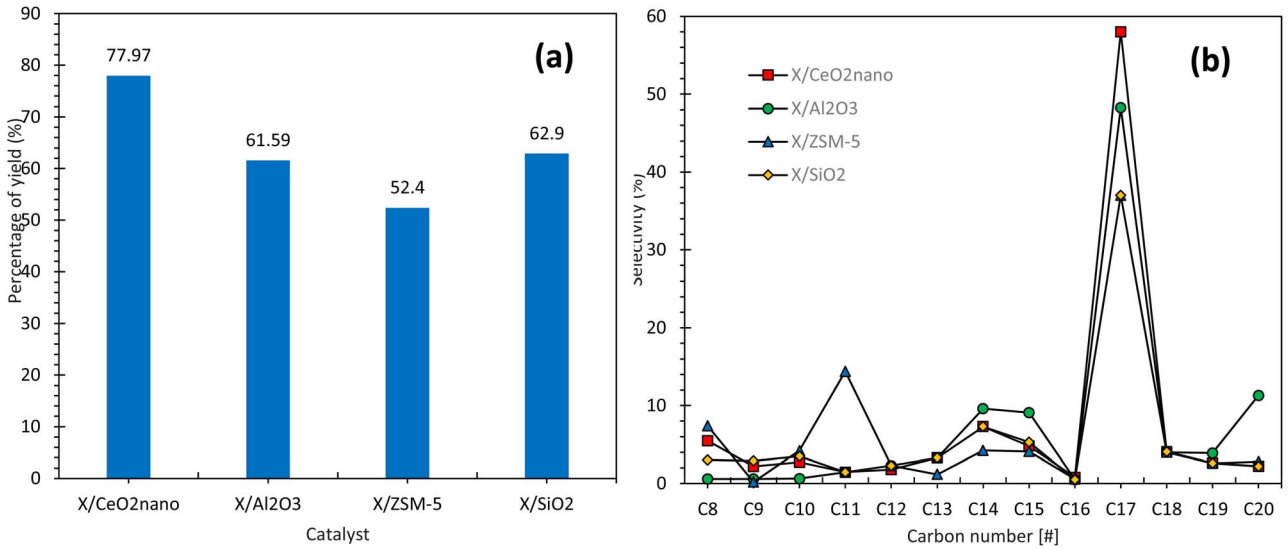

Fig. 5 (a) Hydrocarbon yield and (b) hydrocarbon distribution of the liquid deoxygenated product catalysed by NiO–MoO_2 (*x*) supported onto various materials: CeO_2, Al_2O_3, ZSM-5 and SiO_2 (reaction conditions: 340 °C, 10 mbar, 15 wt%, 1 h, and 400 rpm).

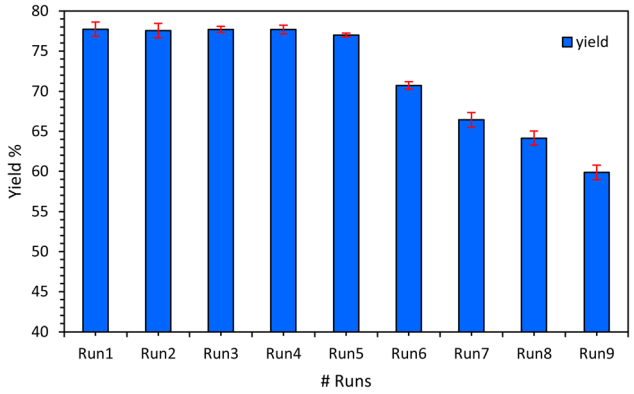

Fig. 6 Effect of catalyst reusability on the deoxygenation of triolein over NiO–MoO_2/CeO_2 under optimum reaction conditions.

reaction is discussed. The deoxygenation activity can be arranged in the order of 1 h > 0.5 h > 1.5 h > 2 h. It had found that the hydrocarbon yield increased proportionally with the reaction time, but the yield dropped as the reaction time prolonged >1.5 h. The reduction of hydrocarbon yield at a longer reaction time is caused by the occurrence of undesirable side reactions (polymerisation and cracking) on the deoxygenated liquid product into lighter fractions (gaseous product).[36,37] Similar trends were observed for the formation of *n*-C_{17}. The *n*-C_{17} selectivity gradually reduced at a longer reaction time, meaning that the cracking activity predominated at a longer reaction time. Indeed, a noticeable amount of cracking products (*n*-C_8) was also detected at 2 h. Therefore, it is strongly affirmed that a longer reaction time results in profound cracking effects than the decarboxylation/decarbonylation activity. Overall, the optimum hydrocarbon yield (77%) and *n*-C_{17} selectivity (58%) can be obtained over 15 wt% of catalyst loading, at 340 °C within 1 h reaction time using the NiO–MoO_2/CeO_2 catalyst.

Fig. 3(e and f) show the effect of the reaction time (0.5–2 h) on the catalytic deoxygenation reaction and product selectivity at 340 °C, 5 wt% catalyst loading, under partial vacuum conditions of 10 mbar reaction pressure, and 400 rpm stirring rate. Based on the result, the highest yield of total hydrocarbon (77.97%) and selectivity towards C_{17} (36.7%) were obtained at 1 h reaction time. The catalytic activity performance followed the order of 1 h > 0.5 h > 1.5 h > 2 h. Therefore, 1 h is the best time of reaction due to the highest percentage of yield and C_{17} selectivity compared to other reaction times. Prolonged time led to lower hydrocarbon yields because after the optimum time, further hydrocarbon cracking will occur and the yield of diesel will decline.[38–40]

3.3.1 Effect of promoters on the yields and selectivity of the product fraction. Fig. 4a and b show the hydrocarbon yield and *n*-C_{17} selectivity for the deoxygenation catalysed by NiO–MoO_2-supported CeO_2 with different Ni/Mo ratios (5/15, 10/10, and 15/5). The results showed that the 10% NiO–10% MoO_2-based catalyst gave the highest hydrocarbon yield (77%), whereas the lowest yield (40%) was obtained from the 15% NiO–5% MoO_2-based catalyst. The hydrocarbon activity followed the order of 10% NiO–10% MoO_2 > 5% NiO–15% MoO_2 > 15% NiO–5% MoO_2. Interestingly, the Mo-rich catalyst was found to be superior towards the deoxygenation activity compared to the Ni-rich catalyst. The Ni-rich catalyst favoured cracking and yielded more gaseous products.[41] Based on the results in Fig. 4b, the *n*-C_{17} selectivity was predominated using 10% NiO–10% MoO_2 with a selectivity close to ~58%. The *n*-C_{17} selectivity increased in the order of 10% NiO–10% MoO_2 > 15% NiO–5% MoO_2 > 5% NiO–15% MoO_2. The high *n*-C_{17} selectivity by the 10% NiO–10% MoO_2 catalyst suggested that the incorporation of the balance amount of Ni and Mo positively minimised the cracking affinity of Ni species. Notably, the 5% NiO–15% MoO_2 catalyst exhibited the lowest *n*-C_{17} selectivity, suggesting that the Mo-rich catalyst negatively interfered with the active sites and led to the deterioration of C–O bond cleavage rate. Hence, it reduced the formation of desired deoxygenated products. Overall, 10% NiO–10% MoO_2-supported CeO_2 was found to be effective in converting triolein to a high-quality diesel-range fuel.

3.3.2 Comparison of different supports on the deoxygenation activity of triolein. Fig. 5a and b display the results of triolein deoxygenation over NiO–MoO_2 supported on various catalyst supports. The catalyst exhibited markedly different catalytic performances, confirming that the catalytic activity and *n*-C_{17} selectivity were affected by the catalyst support. NiO–MoO_2/CeO_2 exhibited the highest hydrocarbon yield (77%) and *n*-C_{17} selectivity (58%) when compared to other catalysts. The hydrocarbon yield for the catalysed deoxygenation followed the order of NiO–MoO_2/CeO_2 > NiO–MoO_2/Al_2O_3 ~ NiO–MoO_2/SiO_2 > NiO–MoO_2/ZSM-5. The trends for *n*-C_{17} hydrocarbons selectivity appeared to follow the order of NiO–MoO_2/CeO_2 > NiO–MoO_2/Al_2O_3 > NiO–MoO_2/SiO_2 ~ NiO–MoO_2/ZSM-5. Similarly, NiO–MoO_2/CeO_2 showed the highest *n*-C_{17} selectivity and NiO–MoO_2/ZSM-5 was the lowest. In addition, NiO–MoO_2/ZSM-5 exhibited a noticeable amount of light fractions (*n*-C_8, *n*-C_{10} and *n*-C_{11}). According to the literature, the high cracking activity of the ZSM-5-supported catalyst was attributed to the presence of rich Brønsted acidic sites on a ZSM-5 support.[12] In summary, CeO_2 can be considered as a promising catalyst support to remove the oxygenate species *via* decarboxylation/decarbonylation reactions.

The reusability performance of the NiO–MoO_2/CeO_2 catalyst in the deoxygenation of triolein provides a crucial assessment of its stability and practical applicability in repeated reaction cycles. As shown in Fig. 6, the catalyst demonstrated high initial activity during the first cycle, achieving significant deoxygenation efficiency and producing hydrocarbons with desirable selectivity, which underscores the strong synergistic effect between NiO, MoO_2, and the CeO_2 support in creating active sites and oxygen vacancies. This high activity can be attributed to the effective interaction between nickel and molybdenum oxides, which promote hydrogenolysis and deoxygenation pathways, while CeO_2 plays a vital role in oxygen storage–release capacity, thereby enhancing the removal of oxygenated species. However, subsequent cycles revealed a progressive decline in activity, suggesting partial deactivation of the catalyst upon reuse. This decrease in catalytic efficiency is commonly associated with several deactivation mechanisms, including coke

Table 3 Comparison study of the reported catalysts and their deoxygenation performance under solvent-free conditions

Feedstock	Main operating conditions	Catalyst	Catalyst preparation method	Liquid yield (%)	Remark	Reference
Triolein	100 °C (synthesis), reaction at mild HDO conditions	NiMo@SAPO-11 (Ni/Mo = 3 : 1)	*In situ* synthesis (microwave-assisted, mild conditions)	86.5 (octadecane selectivity), 100% conversion	MoOx provides oxygen vacancies; excellent selective HDO to diesel-range paraffins	42
Calophyllum inophyllum oil	300–475 °C, solvent-free DO	Mesoporous aluminosilicate (nanocellulose-templated)	Sol–gel + hydrothermal, NCC templating	50.77 (liquid yield), 95.98% conversion	Al-MS (0.25) showed best performance; high selectivity (60.27%) to *n*-C_{15} + C_{17}	43
Palm fatty acid distillate (PFAD)	280–360 °C, 1–5 h, N_2 flow, 1–7 wt% catalyst	Ni/MOF-Cr_2O_3 (Ni-doped pyrolyzed MIL-101)	Wet impregnation + calcination (600 °C, N_2), reduction in H_2	93 hydrocarbon yield, 91% C_{15} + C_{17} selectivity	14Ni/MOF-Cr_2O_3 most effective; high stability and regenerability	44
Triolein	500 °C calcination of TiO_2; DO without external H_2	Mesoporous TiO_2 (M500)	Sol–gel, calcination at 500 °C	76.9 conversion, 78.9 hydrocarbon selectivity	*In situ* H_2 generation; Lewis acidity and mesoporosity enhanced selectivity	7
Triolein	380 °C, 2 h, H_2-free	Ni–Y (transition metal oxides on zeolite Y)	Wet impregnation	76.21 conversion, 84.28 HC selectivity, 92.61 diesel-range	Ni–Y best performer due to Brønsted/Lewis balance; H_2-free DO route	45
Triolein	380 °C, solvent-free, H_2-free	Ni/HMS (10 wt%)	Impregnation onto mesoporous HMS	92.5 conversion, 95.2 selectivity	Ni/HMS synergy (Si–O–Ni bonds); superior dispersion of NiO	46
Triolein	H_2-free DO, mild atmospheric	Fe–Ni/HMS (10 $Fe_{40}Ni$)	Incipient wetness impregnation	96.1 conversion, 91.8 selectivity (C_8–C_{20})	Synergistic Fe–Ni phases (NiO + $NiFe_2O_4$) enhanced acidity & selectivity	46
Triolein	350 °C, 45 min, 5 wt% catalyst, 10 mbar	Co–CaO, W–CaO (waste clamshell-derived)	Waste-shell CaO support, metal oxide impregnation	32% (Co–CaO), 22% (W–CaO) to C_8–C_{17} hydrocarbons	Co–CaO best; gasoline selectivity up to 84%	47
Palm stearin (triglycerides)	350–375 °C, 34 bar H_2, solvent (hexadecane), 1 : 1 reactant : solvent ratio	Ni/ZrO_2	Incipient wetness impregnation	87.75–91.42	High conversion (~98–100%); Ni/ZrO_2 competitive with Pd/C; solvent and temperature strongly influence yield	48
Stearic acid	Up to 900 °C (calcination), batch deoxygenation	Fe_1Ni_3/AC	Co-impregnation, calcination at 900 °C	94 (C_{17} selectivity), 99 conversion	FeNi alloy synergy reduces activation energy; better than noble metals	49
Oil-based drill cuttings (OBDCs)	Pyrolysis 400–700 °C, catalyst : OBDC ratio 1 : 1–10 : 1	FA-ZSM-5, LM-CaO (waste-derived)	Synthesized from fly ash & industrial waste	Hydrocarbons up to 91.09% (C_5–C_{22})	Catalysts reduce oxygenates/PAHs, enhance diesel/gasoline fractions	50
Fatty acid methyl esters (FAME)	350 °C, 2 MPa H_2, solvent-free	MnFeCoNiCu/C	*In situ* preparation	100% conversion; ~51% green diesel	Produces both bio-jet (C_8–C_{16}) and diesel (C_{17}–C_{22}) in one step	51
Food waste oil fraction	Enzymatic decarboxylation at mild conditions (lipase + CvFAP, biphasic)	Enzyme (lipase + CvFAP)	Enzymatic, biphasic (petroleum ether)	42.2 conversion in 1 h (palmitic acid); hydrocarbon generation rate 1.7 mM h^{-1}	Mild, green process; coupled with anaerobic digestion for CH_4	52
Palm oil	Hydrothermolysis, 400 °C, 3 h, no external H_2	Ni/HUSY-AW (acid-treated zeolite support)	Ni impregnation + acid dealumination	61.54 (alkanes); 35.17 aromatics	*In situ* H_2 from water reforming; sustainable SAF route	53
Sustainable oils (triglycerides)	200–350 °C, inert N_2, deoxygenation	Co–Ni/MIL-101(Fe) MOF	MOF reconstruction, controlled Co–Ni loading	98.84 yield, 85.43 *n*-C15 selectivity	High acid/base site density; hydrogen-free deoxygenation	54
Waste cooking oil	NiO/MAS (Si/Al ratio 30–60), 300–350 °C	NiO/mesoporous aluminosilicate	Natural template (*Sapindus rarak* extract) + impregnation	~96 selectivity to C_8–C_{20}	Si/Al ratio tunes acidity; avoids excessive cracking	55

Table 3 (*Contd.*)

Feedstock	Main operating conditions	Catalyst	Catalyst preparation method	Liquid yield (%)	Remark	Reference
n-Hexadecane (model)	360 °C, hydrocracking	Cat-*x*Ni (Ni-doped Y zeolite + ASA)	*In situ* Ni doping + impregnation	65.4 C_8–C_{12} fraction	Small crystal NiY improves balance of acidity & metal function	56
Waste cooking oil & stearic acid	Batch & continuous (trickle-bed), HDO, 300–350 °C	Mo_2C/CNF	Mo_2C supported on carbon nanofibers	86 (mol%)	Direct HDO favored; high-quality green diesel	57
Triolein	Semi-batch reactor	NiO–MoO_2/CeO_2	Impregnation	77%	Under vacuum condition and free hydrogen	Current work

deposition on the active surface, sintering of metal particles at elevated reaction temperatures, or poisoning of active sites due to strong adsorption of reaction intermediates. The reduction in performance after multiple cycles indicates that carbonaceous deposits might block the active Ni–Mo sites and decrease the availability of surface oxygen vacancies, thereby hindering the catalyst's ability to sustain efficient deoxygenation reactions. Despite this decline, the catalyst retained a notable portion of its initial activity, reflecting a reasonable degree of durability and reusability, which is advantageous when compared to conventional deoxygenation catalysts that often exhibit more rapid deactivation. Moreover, the retention of activity in multiple runs accentuates the structurally robust nature of the CeO_2 support that can stabilize Ni and Mo species against extensive sintering and endow redox functionality to partially hinder deactivation. The trend, as observed, strongly indicates that regeneration approaches like oxidative treatment to clean up surface coke or cyclic reactivation of metal oxides can reinstate catalytic performance and prolong its working lifespan. From a wider viewpoint, the reusability performance of the NiO–MoO_2/CeO_2 is indicative of the prospects as well as the challenges in crafting productive catalysts to produce green fuel. On the one hand, the material exhibits encouraging activity, selectivity, as well as moderate tolerance to deactivation that is vital to practicality. On the other hand, the progressive diminution throughout cycles is indicative of the requirement to improve the catalyst structure—perhaps through optimal techniques towards the synthesis to aid in the dispersion of active phases, doping with promoters to enhance carbon deposition resistance, or engineering hierarchical pore structure to aid product diffusivity while suppressing coke buildup. Overall, the reusability trial endorses the characterization of NiO–MoO_2/CeO_2 as an excellent contender towards the deoxygenation of triglyceride feedstocks like triolein, while also underlining that additional study into regeneration as well as stabilization approaches will form part of the requirement to realize long-working viability in commercial biofuel production.

The comparison between previous works and this study identifies both the accretive progress in deoxygenation catalysis, and this work has distinct novelty. Preceding studies utilized various catalytic systems, namely NiMo@SAPO-11, mesoporous aluminosilicate, composites of Ni/MOF, and transition metal oxides over supported zeolites, mostly under solvent-free or hydrogen-free conditions. Such systems tended to yield high conversion and selectivity, particularly when state-of-the-art supports enhanced acidity, oxygen vacancy induction, or *in situ* hydrogen generation. For example, clamshell-derived CaO enabled energy efficiency through waste valorization, while fly ash-modified ZSM-5 demonstrated attempts to incorporate sustainability through waste valorization. Nonetheless, most systems still suffered from recurrent issues such as elevated operating temperatures, energy-intensive hydrogen dependency, and complicated template or synthetic protocols, all of which limit scalability in the industrially relevant environment.

The current study presents NiO–MoO_2/CeO_2 as a semi-batch vacuum-established catalytic platform under hydrogen-free conditions, breaking with the usual high-pressure hydrogen-based approach. Through the combination of NiO and MoO_2 with CeO_2, redox activity and oxygen mobility are leveraged to enable deoxygenation, while vacuum operation suppresses uncontrolled secondary cracking. A liquid yield of 77% under relatively modest conditions is indicative of practical promise. All the same, as this study stands against the background of previous studies as well, it is important to note that this study has methodological limitations. Unlike continuous-flow systems that more closely mirror industrial operation, this semi-batch arrangement presents limitations to direct scaling. Second, while simplicity in impregnation avoids elaborate synthesis, this may also mean less good dispersion control compared to sophisticated templating or sol–gel approaches that are used in calibration studies, possibly giving rise to long-term stability scatter. Lastly, while external hydrogen elimination is an advantage, this study has still not fully accounted for deactivation pathways in the catalyst in the form of, *e.g.*, coking that is still the weak link in hydrogen-free operation.

The significance of this contribution is striking a balance between novelty and feasibility. Initially, it moves the field forward by introducing an economically feasible deoxygenation approach that decreases the dependence on hydrogen, the significant cost as well as environmental liability in biofuel upgrading. Second, it provides a simpler synthesis path than

complex templated schemes, though in the name of finesse that may have to suffer in terms of easier textural control. Third, it is in line with circular economy thinking by pursuing the kind of pathway that is not only large scale but also sustainable. Overall, though the current effort may sacrifice some structural finesse in comparison to previous catalysts (Table 3), it represents an important stride towards industrially useful, low-cost, as well as environmentally friendly hydrocarbon fuel production from triglyceride feedstocks like triolein.

4. Conclusion

In the present work, the NiO–MoO_2/CeO_2 catalyst had successfully converted triolein into a desired deoxygenated hydrocarbon product (*n*-C_{17}) under partial vacuum and solvent-free conditions. The obtained results revealed that the catalytic performance of NiO–MoO_2/CeO_2 enormously depends on its acid–base character. The rich acid–base character was beneficial for promoting the oxygenate removal activity exclusively *via* decarboxylation/decarbonylation pathways. The effectiveness of this binary metal oxide–supported CeO_2 is also associated with the excellent synergistic interaction between Ni and Mo on the CeO support. Based on the optimisation study, the optimum hydrocarbon yield (77%) and *n*-C_{17} selectivity (58%) can be obtained over 15 wt% of catalyst loading, 340 °C within 1 h of reaction time. A study on the effect of Ni and Mo concentrations revealed that the Mo-rich and Ni-rich catalysts negatively affected the C–O bond cleavage. Based on the catalyst support comparison, CeO_2 was found to be promising for the production of diesel-range fuels *via* solvent-free catalytic deoxygenation of triolein.

Conflicts of interest

There are no conflicts to declare.

Data availability

All the data will be available from the corresponding authors upon request.

Acknowledgements

This research was financially supported by the Ministry of Higher Education, Malaysia, for niche area research under the Higher Institution Centre of Excellence (HICoE) program (JPT(BKPI)1000/016/018/28 Jld.3(2) & NANOCAT-2024E), and the authors would like to acknowledge the financial support from Universiti Kebangsaan Malaysia through the Research University Grant (TRUKM: UKM-TR2024-15) and the DIP 2.0 Grant (DIP-2024-027).

References

1 S. Ki, J. Young, H. Lee, T. Yum, Y. Kim and J. Kim, *Appl. Energy*, 2014, **116**, 199–205.
2 D. de L. A. D. Pereyra, I. B. Rueger, P. A. M. de A. Barbosa, F. S. Peiter, D. M. da Silva Freitas and E. L. C. de Amorim, *J. Chem. Eng.*, 2020, **37**, 653–660.
3 C. A. Ortiz-Bravo, C. H. Zandonai, M. H. N. Olsen-Scaliante and N. R. C. Fernandes, *J. Chem. Eng.*, 2020, **37**, 691–701.
4 N. Asikin-Mijan, N. A. Rosman, G. AbdulKareem-Alsultan, M. S. Mastuli, H. V. Lee, N. Nabihah-Fauzi, I. M. Lokman, F. A. Alharthi, A. A. Alghamdi, A. A. Aisyahi and Y. H. Taufiq-Yap, *Process Saf. Environ. Prot.*, 2020, **142**, 336–349.
5 G. W. Huber, P. O'Connor and A. Corma, *Appl. Catal., A*, 2007, **329**, 120–129.
6 C. Miao, O. Marin-Flores, S. D. Davidson, T. Li, T. Dong, D. Gao, Y. Wang, M. Garcia-Pérez and S. Chen, *Fuel*, 2016, **166**, 302–308.
7 L. E. Oi, M. Y. Choo, H. V. Lee, Y. H. Taufiq-Yap, C. K. Cheng and J. C. Juan, *Int. J. Hydrogen Energy*, 2020, **45**, 11605–11614.
8 X. Y. Ooi, L. E. Oi, M. Y. Choo, H. C. Ong, H. V. Lee, P. L. Show, Y. C. Lin and J. C. Juan, *Fuel Process. Technol.*, 2019, **194**, 106120.
9 S. De and R. Luque, *Biofuel Res. J.*, 2014, **1**, 107–109.
10 H. Imai, T. Kimura, K. Terasaka, X. Li, K. Sakashita, S. Asaoka and S. S. Al-Khattaf, *Catal. Today*, 2018, **303**, 185–190.
11 D. Kubička and L. Kaluža, *Appl. Catal., A*, 2010, **372**, 199–208.
12 H. Chen, Q. Wang, X. Zhang and L. Wang, *Appl. Catal., B*, 2015, **166–167**, 327–334.
13 A. I. Hussain, A. M. Aitani, M. Kubů, J. Čejka and S. Al-Khattaf, *Fuel*, 2016, **167**, 226–239.
14 N. Arun, J. Maley, N. Chen, R. Sammynaiken, Y. Hu and A. K. Dalai, *Catal. Today*, 2017, **291**, 153–159.
15 M. Grilc and B. Likozar, *Chem. Eng. J.*, 2017, **330**, 383–397.
16 H. Shi, J. Chen, Y. Yang and S. Tian, *Fuel Process. Technol.*, 2014, **118**, 161–170.
17 Y. Lin, C. Zhang, M. Zhang and J. Zhang, *Energy Fuels*, 2010, **24**, 5686–5695.
18 B. Peng, X. Yuan, C. Zhao and J. A. Lercher, *J. Am. Chem. Soc.*, 2012, **134**, 9400–9405.
19 H. S. Roh, I. H. Eum and D. W. Jeong, *Renewable Energy*, 2012, **42**, 212–216.
20 O. Nagashima, S. Sato, R. Takahashi and T. Sodesawa, *J. Mol. Catal. A: Chem.*, 2005, **227**, 231–239.
21 V. A. Yakovlev, S. A. Khromova, O. V. Sherstyuk, V. O. Dundich, D. Y. Ermakov, V. M. Novopashina, M. Y. Lebedev, O. Bulavchenko and V. N. Parmon, *Catal. Today*, 2009, **144**, 362–366.
22 N. Aliana-Nasharuddin, N. Asikin-Mijan, G. Abdulkareem-Alsultan, M. I. Saiman, F. A. Alharthi, A. A. Alghamdi and Y. H. Taufiq-Yap, *RSC Adv.*, 2019, **10**, 626–642.
23 M. Safa Gamal, N. Asikin-Mijan, M. Arumugam, U. Rashid and Y. H. Taufiq-Yap, *J. Anal. Appl. Pyrolysis*, 2019, **144**, 104690.
24 W. N. Adira Wan Khalit, T. S. Marliza, N. Asikin-Mijan, M. S. Gamal, M. I. Saiman, M. L. Ibrahim and Y. H. Taufiq-Yap, *RSC Adv.*, 2020, **10**, 37218–37232.
25 E. Kumar, P. Selvarajan and K. Balasubramanian, *Recent Res. Sci. Technol.*, 2010, **2**, 37–41.

26 Y. C. Wong, Y. P. Tan, Y. H. Taufiq-Yap, I. Ramli and H. S. Tee, *Fuel*, 2015, **162**, 288–293.
27 S. Rakshit, S. Ghosh, S. Chall, S. S. Mati, S. P. Moulik and S. C. Bhattacharya, *RSC Adv.*, 2013, **3**, 19348–19356.
28 J. I. López-Pérez, E. O. Ortiz-Quiles, K. Habiba, M. Jiménez-Rodríguez, B. R. Weiner and G. Morell, *ISRN Electrochem.*, 2014, **2014**, 1–12.
29 W. Xie, H. Peng and L. Chen, *Appl. Catal., A*, 2006, **300**, 67–74.
30 R. Ding, Y. Wu, Y. Chen, J. Liang, J. Liu and M. Yang, *Chem. Eng. Sci.*, 2015, **135**, 517–525.
31 B. Peng, C. Zhao, S. Kasakov, S. Foraita and J. A. Lercher, *Chem.–Eur. J.*, 2013, **19**, 4732–4741.
32 H. Song, N. Wang, H. L. Song and F. Li, *Catal. Commun.*, 2015, **59**, 61–64.
33 N. Asikin-Mijan, J. C. Juan, Y. H. Taufiq-Yap, H. C. Ong, Y. C. Lin, G. AbdulKareem-Alsultan and H. V. Lee, *Catal. Commun.*, 2023, **182**, 106741.
34 G. Abdulkareem-Alsultan, N. Asikin-Mijan, L. K. Obeas, R. Yunus, S. Z. Razali, A. Islam and Y. Hin Taufiq-Yap, *Chem. Eng. J.*, 2022, **429**, 132206.
35 K. C. Kwon, H. Mayfield, T. Marolla, B. Nichols and M. Mashburn, *Renewable Energy*, 2011, **36**, 907–915.
36 N. Asikin-Mijan, J. M. Ooi, G. AbdulKareem-Alsultan, H. V. Lee, M. S. Mastuli, N. Mansir, F. A. Alharthi, A. A. Alghamdi and Y. H. Taufiq-Yap, *J. Clean. Prod.*, 2020, **249**, 119381.
37 S. T. A. Maciel, J. H. C. Reis, G. F. da Silva and L. dos Santos Freitas, *J. Chem. Eng.*, 2021, **38**, 123–131.
38 M. M. X. Lum, K. H. Ng, S. Y. Lai, A. R. Mohamed, A. G. Alsultan, Y. H. Taufiq-Yap, M. K. Koh, M. A. Mohamed, D. V. N. Vo, M. Subramaniam, K. S. Mulya and N. Imanuella, *Process Saf. Environ. Prot.*, 2023, **176**, 580–604.
39 H. K. Faten, A. Salmiaton, R. M. H. R. Shahruzzaman, R. Omar and A. G. Alsultsan, *Bull. Chem. React. Eng. Catal.*, 2017, **12**, 81–88.
40 K. A. Samawi, S. J. Abdulrazzaq, M. Zorah, M. Al-Bahrani, H. A. M. A. Mahmoud, G. Abdulkareem-Alsultan, A. G. Taki and M. F. Nassar, *J. Solid State Chem.*, 2024, **334**, 124690.
41 N. Asikin-Mijan, H. V. Lee, G. Abdulkareem-Alsultan, A. Afandi and Y. H. Taufiq-Yap, *J. Clean. Prod.*, 2017, **167**, 1048–1059.
42 D. Zheng, L. Li and S. Yu, *Mol. Catal.*, 2025, **579**, 1–12.
43 S. Jovita, A. T. Melenia, E. Santoso, R. Subagyo, R. Tamim, N. Asikin-Mijan, H. Holilah, H. Bahruji, R. E. Nugraha, A. A. Jalil, H. Tehubijuluw, M. Ulfa and D. Prasetyoko, *Renewable Energy*, 2025, **250**, 1–17.
44 H. Chang, H. V. Lee, Y. H. Taufiq-Yap, G. Abdulkareem-Alsultan and S. Seenivasagam, *Renewable Energy*, 2025, **238**, 121882.
45 M. Y. Choo, L. E. Oi, T. C. Ling, E. P. Ng, Y. C. Lin, G. Centi and J. C. Juan, *J. Anal. Appl. Pyrolysis*, 2020, **147**, 104797.
46 S. Zulkepli, N. A. Rahman, H. Voon Lee, C. Kui Cheng, W. H. Chen and J. Ching Juan, *Energy Convers. Manag.*, 2022, **273**, 116371.
47 N. Asikin-Mijan, H. V. Lee, J. C. Juan, A. R. Noorsaadah, G. Abdulkareem-Alsultan, M. Arumugam and Y. H. Taufiq-Yap, *J. Anal. Appl. Pyrolysis*, 2016, **120**, 110–120.
48 M. Lalitpattarakit, C. Prapainainar, N. Hongloi, P. Ounsuk, K. Sudsakorn, A. Seubsai, P. Sureeyatanapas, W. Kiatkittipong, S. Wongsakulphasatch, S. Assabumrungrat and P. Prapainainar, *Chem. Eng. J.*, 2025, **508**, 161125.
49 K. B. Tan, Y. Qiu, Y. Li, B. Chen, L. Xia, D. Cai, S. Ali, J. Huang and G. Zhan, *Mol. Catal.*, 2024, **565**, 114361.
50 S. Vichaphund, P. Wimuktiwan, K. Soongprasit, V. Sricharoenchaikul and D. Atong, *Process Saf. Environ. Prot.*, 2025, **199**, 107244.
51 K. Wu, Q. Yao, D. Wang, H. Huang, J. Lin, Q. Fan, Y. Wu, J. Duan, J. Zheng, Y. Ye, D. Wang, Y. Huang, J. Jiang and Z. Zheng, *Energy Convers. Manag.*, 2024, **318**, 118875.
52 X. Guo, A. Xia, F. Li, Y. Huang, X. X. Zhu, W. Zhang, X. X. Zhu and Q. Liao, *Energy Convers. Manag.*, 2024, **308**, 118409.
53 S. Sedtabute, T. Vitidsant and C. Ngamcharussrivichai, *Energy Convers. Manag.*, 2025, **331**, 119679.
54 A. F. Mohammed, G. Abdulkreem-Alsultan, L. K. Obeas, N. Asikin-Mijan, S. Samidin, N. Azri, W. N. A. W. Khalit, M. F. Nassar, H. V. Lee, S. Y. Lai, M. Y. Tan and Y. H. Taufiq-Yap, *J. Alloys Compd.*, 2025, **1039**, 182906.
55 S. Jovita, N. Nadhifah, R. Subagyo, R. Tamim, E. P. Ramdhani, H. Holilah, N. Asikin-Mijan, H. Bahruji, R. E. Nugraha, A. A. Jalil, S. Suprapto and D. Prasetyoko, *Biomass Bioenergy*, 2025, **200**, 107977.
56 J. Sun, X. Wang, Q. Wei and Y. Zhou, *J. Fuel Chem. Technol.*, 2024, **52**, 775–789.
57 A. Muñoz-Arjona, A. Ayala-Cortés, C. Di Stasi, D. Torres, J. L. Pinilla and I. Suelves, *Chem. Eng. J.*, 2025, **502**, 158503.